Abstracta

Ano XX - N. 05

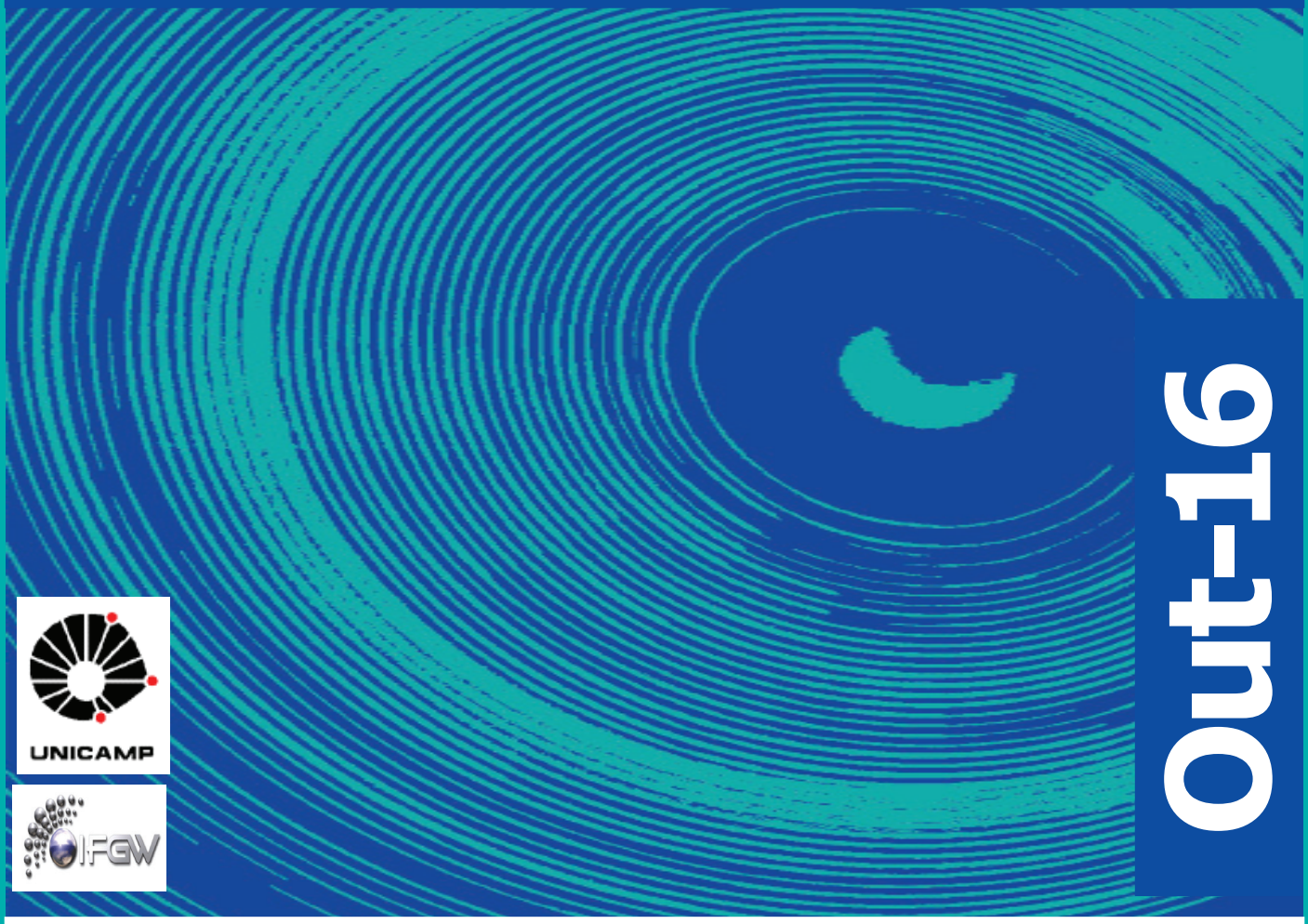

Out-16

UNICAMP

IFGW

Artigos publicados - P217-2016 à P272-2016

Eventos publicados - P273-2016 à P274-2016

Patentes - Pa001-2016 à Pa003-2016

Livro Publicado - L003-2016

Defesas de Dissertações do IFGW - D022-2016 à D023-2016

Defesas de Teses do IFGW - T012-2016 à T013-2016

Artigos publicados

[P217-2016] "Cerebral Regulation in Different Maximal Aerobic Exercise Modes"

Pires, F. O.; **dos Anjos, C. A. S.*; Covolan, R. J. M.***; Pinheiro, F. A.; Gibson, A. St C.; Noakes, T. D.; Magalhaesi, F. H.; Ugrinowitsch, C.

We investigated cerebral responses, simultaneously with peripheral and ratings of perceived exertion (RPE) responses, during different VO2MAX-matched aerobic exercise modes. Nine cyclists (VO2MAX of 57.5 +/- 6.2 ml.kg(-1).min(-1)) performed a maximal, controlled-pace incremental test (MIT) and a self-paced 4 km time trial (TT4km). Measures of cerebral (COX) and muscular (MOX) oxygenation were assessed throughout the exercises by changes in oxy-(O(2)Hb) and deoxy-hemoglobin (HHb) concentrations over the prefrontal cortex (PFC) and vastus lateralis (VL) muscle, respectively. Primary motor cortex (PMC) electroencephalography (EEG), VL, and rectus femoris EMG were also assessed throughout the trials, together with power output and cardiopulmonary responses. The RPE was obtained at regular intervals. Similar motor output (EMG and power output) occurred from 70% of the duration in MIT and TT4km, despite the greater motor output, muscle deoxygenation (down arrow MOX) and cardiopulmonary responses in TT4km before that point. Regarding cerebral responses, there was a lower COX (1, O(2)Hb concentrations in PFC) at 20, 30, 40, 50 and 60%, but greater at 100% of the TT4km duration when compared to MIT The alpha wave EEG in PMC remained constant throughout the exercise modes, with greater values in TT4km. The RPE was maximal at the endpoint in both exercises, but it increased slower in TT4km than in MIT. Results showed that similar motor output and effort tolerance were attained at the closing stages of different VO2MAX-matched aerobic exercises, although the different disturbance until that point. Regardless of different COX responses during most of the exercises duration, activation in PMC was preserved throughout the exercises, suggesting that these responses may be part of a centrally coordinated exercise regulation.

FRONTIERS IN PHYSIOLOGY 7, 253, 2016. DOI: 10.3339/fphys.2016.00253

[P218-2016] "Coevolution in sexually reproducing populations of predators and prey"

Nagai, M. E.; **de Aguiar, M. A. M.***

The dynamics of coevolution is a spatio-temporal process that cannot be understood by mean field approximations, where populations are considered well mixed and interactions are random. This intrinsic characteristic makes comprehensive empirical studies difficult and computer simulations can help to understand the interplay between the many components of the interactions. Here we created an individual-based model to study the coevolution of sexually reproducing populations of prey and predators that engage in an arms race. The phenotype interface of the interaction is a defensive trait for the prey and a counter-defensive one for the predator, both having costs that decrease reproduction chances. The simulations captured several features of natural systems, such as oscillations of the phenotypes levels and abundances. More importantly, the simulations show that local depletion of prey by predators with high levels of counter-defenses followed by recolonization by less defensive prey is a key mechanism that regulates the arms race and the spatio-temporal distribution of phenotypes, creating mismatches similar to those observed in natural systems.

ECOLOGICAL MODELLING 337, 168-175, 2016. DOI: 10.1016/j.ecolmodel.2016.06.017

[P219-2016] "Combining state-of-the-art experiment and ab initio calculations for a better understanding of the interplay between valence, magnetism and structure in Eu compounds at high pressure"

Souza-Neto, N. M.; Haskel, D.; **dos Reis, R. D.*; Gandra, F. C. G.***

We describe how first principle calculations can play a key role in the interpretation of X-ray absorption near-edge structure (XANES) and X-ray magnetic circular dichroism (XMCD) spectra for a better understanding of emergent phenomena in condensed matter physics at high applied pressure. Eu compounds are used as case study to illustrate the advantages of this methodology, ranging from studies of electronic charge transfer probed by quadrupolar and dipolar contributions, to accurately determining electronic valence, and to inform about the influence of pressure on RKKY interactions and magnetism. This description should help advance studies where the pressure dependence of XANES and XMCD data must be tackled with the support of theoretical calculations for a proper understanding of the electronic properties of materials.

HIGH PRESSURE RESEARCH 36[3]SI, 360-370, 2016. DOI: 10.1080/08957959.2016.1212025

[P220-2016] "Computational investigation on CO2 adsorption in titanium carbide-derived carbons with residual titanium"

Difan Z.; Michael R. D.; Tao Liang; **Fonseca, A. F.*,** Ying Wu; Krista S. W.; David S. S.; Amir H. F.; Suresh K. B.; Susan B. S.

We develop a new approach for modeling titanium carbide derived-carbon (TiC-CDC) systems with residual titanium by the generation of modified atomistic structures based on a silicon carbide derived-carbon (SiC-CDC) model and the application of weighted combinations of these structures. In our approach, the original SiC-CDC structure is modified by (i) removing carbon, (ii) adding carbon and (iii) adding titanium. The new atomic scale carbide-derived carbon (CDC) structures are investigated using classical molecular dynamics simulations, and their pure CO2 adsorption isotherms are calculated using grand canonical Monte Carlo simulations. The system of TiC-CDC with residual titanium is modeled as weighted combinations of pure carbon CDC structures, CDC structures with titanium and a TiC crystalline structure. Our modeling is able to produce both structural properties and adsorption isotherms in accordance with experimental data. The fraction of different models in the systems successfully reflects the structural differences in various experimental TiC-CDC samples. The modeling also suggests that in partially etched TiC-CDC systems, the titanium that may be accessible to CO2 gas at the transitional interface may provide significant interaction sites for CO2 and may lead to more efficient overall gas adsorption.

CARBON 111, 741-751, 2016. DOI: http://dx.doi.org/10.1016/j.carbon.2016.10.037

[P221-2016] "Configuring Electronic States in an Atomically Precise Array of Quantum Boxes"

Nowakowska, S.; Wackerlin, A.; Piquero-Zulaica, I.; Nowakowski, J.; Kawai, S.; Wackerlin, C.; Matena, M.; Nijs, T.; **Fatayer, H.***; Popova, O.; Ahsan, A.; Mousavi, S. F.; Ivas, T.; Meyer, E.; Stohr, M.; Enrique O. J.; Bjork, J.; Gade, L. H.; Lobo-Checa, J.; Jung, T. A.

A 2D array of electronically coupled quantum boxes is fabricated by means of on-surface self-assembly assuring ultimate precision of each box. The quantum states embedded in the boxes are configured by adsorbates, whose occupancy is controlled with atomic precision.

The electronic interbox coupling can be maintained or significantly reduced by proper arrangement of empty and filled boxes.

SMALL 12[28] 3757-3763, 2016. DOI: 10.1002/smll.201600915

[P222-2016] "Controlled 3D Carbon Nanotube Structures by Plasma Welding"

Ozden, S.; **Brunetto, G.***; Karthiselva, N. S.; **Galvao, D. S.***; Roy, A.; Bakshi, S. R.; Tiwary, C. S.; Ajayan, P. M.

3D interconnected carbon nanotubes (CNTs) are synthesized using an industrially scalable spark plasma technique. At high electric field and elevated temperature under sufficient stress the nanotubes are welded together to form a solid block. The detailed spectroscopic and microscopic analyses show successful welding of the CNTs and formation of interconnected networks. The mechanical characteristics of the 3D CNT block show a high stiffness and yield strength. A full atomistic molecular dynamics simulation elucidates the CNT welding mechanism.

ADVANCED MATERIALS INTERFACES 3[13]1500755, 2016. DOI: 10.1002/admi.201500755

[P223-2016] "Cosmological Bounds of Sterile Neutrinos in a S U(3) (C) aSuS U(3) (L) aSuS U(3) (R) aSuU(1) (N) Model as Dark Matter Candidates"

Ferreira, C. P.*; Guzzo, M. M.*; de Holanda, P. C.*

We study sterile neutrinos in an extension of the standard model, based on the gauge group S U(3) (C) aSuS U(3) (L) aSuS U(3) (R) aSuU(1) (N) , and use this model to illustrate how to apply cosmological limits to thermalized particles that decouple while relativistic. These neutrinos, N (a L) , can be dark matter candidates, with a kiloelectron volt mass range arising rather naturally in this model. We analyse the cosmological limits imposed by N (e f f) and dark matter abundance on these neutrinos. Assuming that these neutrinos have roughly equal masses and are not CDM, we conclude that the N (e f f) experimental value can be satisfied in some cases and the abundance constraint implies that these neutrinos are hot dark matter. With this information, we give upper bounds on the Yukawa coupling between the sterile neutrinos and a scalar field, the possible values of the VEV of this scalar field and lower bounds to the mass of one gauge boson of the model.

BRAZILIAN JOURNAL OF PHYSICS 46[4] 453-461, 2016. DOI: 10.1007/s13538-016-0427-2

[P224-2016] "Edge phonons in black phosphorus"

Ribeiro, H. B.; Villegas, C. E. P.; Bahamon, D. A.; **Muraca, D.***; Castro Neto, A. H.; de Souza, E. A. T.; Rocha, A. R.; Pimenta, M. A.; de Matos, C. J. S.

Black phosphorus has recently emerged as a new layered crystal that, due to its peculiar and anisotropic crystalline and electronic band structures, may have important applications in electronics, optoelectronics and photonics. Despite the fact that the edges of layered crystals host a range of singular properties whose characterization and exploitation are of utmost importance for device development, the edges of black phosphorus remain poorly characterized. In this work, the atomic structure and behaviour of phonons near different black phosphorus edges are experimentally and theoretically studied using Raman spectroscopy and density functional theory calculations. Polarized Raman results show the appearance of new modes at the edges of the sample, and their spectra depend on the atomic structure of the edges (zigzag or armchair). Theoretical simulations confirm that the new modes are due to edge phonon states that are forbidden in the bulk, and originated from the lattice termination rearrangements.

NATURE COMMUNICATIONS 7, 12191, 2016. DOI: 10.1038/ncomms12191

[P225-2016] "Electromagnetically induced cross focusing in a four-level atomic medium"

Becerra-Castro, E. M.; **de Araujo, L. E. E.***

We describe cross focusing in a four-level atomic medium under electromagnetically induced transparency. We show that due to the giant Kerr nonlinearity experienced by the atoms, cross focusing between weak signal and probe fields (both fields with intensities below line saturation level) is possible. By applying different intensity masks to the signal field, different lenses (cylindrical, Fresnel, Gaussian) can be induced in the atomic sample. Focusing of the probe beam is analyzed in terms of the excitation parameters (signal Rabi frequency and detuning, as well as optical depth of the atomic medium).

JOURNAL OF THE OPTICAL SOCIETY OF AMERICA B-OPTICAL PHYSICS 33[8]1574-1579, 2016. DOI: 10.1364/JOSAB.33.001574

[P226-2016] "Electron scattering by biomass molecular fragments: useful data for plasma applications?"

Ridenti, M. A.*; Amorim Filho, J.*; Brunger, M. J.; da Costa, R. F.; Varella, M. T. do N.; Bettega, M. H. F.; **Lima, M. A. P.***

Recent data obtained for electron scattering by biomass molecular fragments, indicated that low-energy resonances may have an important role in the de-lignification of biomass through a plasma pretreatment. To support these findings, we present new experimental evidence of the predicted dissociation pathways on plasma treatment of biomass. An important question is how accurate must the experimental and/or the theoretical data be in order to indicate that plasma modelings can be really useful in understanding plasma applications? In this paper, we initiate a discussion on the role of data accuracy of experimental and theoretical electron-molecule scattering cross sections in plasma modeling. First we review technological motivations for carrying out electron-molecule scattering studies. Then we point out the theoretical and experimental limitations that prevent us from obtaining more accurate cross sections. We present a few examples involving biomass molecular fragments, to illustrate theoretical inaccuracies on: resonances positions and widths, electronic excitation, superelastic cross sections from metastable states and due to multichannel effects on the momentum transfer cross sections. On the experimental side we briefly describe challenges in making absolute cross sections measurements with biomass species and radicals. And finally, through a simulation of a N-2 plasma, we illustrate the impact on the simulation due to inaccuracies on the resonance positions and widths and due to multichannel effects on the momentum transfer cross sections.

EUROPEAN PHYSICAL JOURNAL D 70[8], 2016. DOI: 10.1140/epjd/e2016-70272-8

[P227-2016] "Elliptic flow of electrons from heavy-flavour hadron decays at mid-rapidity in Pb-Pb collisions at root s(NN)=2.76 TeV"

Adam, J.; Adamova, D.; Aggarwal, M. M.; Albuquerque, D. S. D.*; **Chinellato, D. D.*; De Souza, R. D.*; Takahashi, J.*;** et al. ALICE Collaboration

The elliptic flow of electrons from heavy-flavour hadron decays at mid-rapidity (|y| < 0.7) is measured in Pb-Pb collisions at TeV with ALICE at the LHC. The particle azimuthal distribution with respect to the reaction plane can be parametrized with a Fourier expansion, where the second coefficient (v (2)) represents the elliptic flow. The v (2) coefficient of inclusive electrons is measured in three centrality classes (0-10%, 10-20% and 20-40%) with the event plane and the scalar product methods in the transverse momentum (p (T)) intervals 0.5-13 GeV/c and 0.5-8 GeV/c, respectively. After subtracting the background, mainly from photon conversions and Dalitz decays of neutral mesons, a positive v (2) of electrons from heavy-flavour hadron decays is observed in all centrality classes, with a maximum significance of 5.9 sigma in the interval 2 < p (T) < 2.5 GeV/c in semi-central collisions (20-40%). The value of v (2) decreases towards more central collisions at low and intermediate p (T) (0.5 < p (T) < 3 GeV/c). The v (2) of electrons from heavy-flavour hadron decays at mid-rapidity is found to be similar to the one of muons from heavy-flavour hadron decays at forward rapidity (2.5 < y < 4). The results are described within uncertainties by model calculations including substantial elastic interactions of heavy quarks with an expanding strongly-interacting medium.

JOURNAL OF HIGH ENERGY PHYSICS 9, 028, 2016. DOI: 10.1007/JHEP09(2016)028

[P228-2016] "Giant and Tunable Anisotropy of Nanoscale Friction in Graphene"

Almeida, C. M.; Prioli, R.; Fragneaud, B.; Cancado, L. G.; Paupitz, R.; **Galvao, D. S.***; De Cicco, M.; Menezes, M. G.; Achete, C. A.; Capaz, R. B.

The nanoscale friction between an atomic force microscopy tip and graphene is investigated using friction force microscopy (FFM). During the tip movement, friction forces are observed to increase and then saturate in a highly anisotropic manner. As a result, the friction forces in graphene are highly dependent on the scanning direction: under some conditions, the energy dissipated along the armchair direction can be 80% higher than along the zigzag direction. In comparison, for highly-oriented pyrolitic graphite (HOPG), the friction anisotropy between armchair and zigzag directions is only 15%. This giant friction anisotropy in graphene results from anisotropies in the amplitudes of flexural deformations of the graphene sheet driven by the tip movement, not present in HOPG. The effect can be seen as a novel manifestation of the classical phenomenon of Euler buckling at the nanoscale, which provides the non--linear ingredients that amplify friction anisotropy. Simulations based on a novel version of the 2D Tomlinson model (modified to include the effects of flexural deformations), as well as fully atomistic molecular dynamics simulations and first--principles density-functional theory (DFT) calculations, are able to reproduce and explain the experimental observations.

SCIENTIFIC REPORTS 6, 31569, 2016. DOI: 10.1038/srep31569

[P229-2016] "Holographic entanglement renormalization of topological insulators"

Wen, X.; Cho, G. Y.; **Lopes, P. L. S.***; Gu, Y.; Qi, X.; Ryu, S.

We study the real-space entanglement renormalization group flows of topological band insulators in (2+1) dimensions by using the continuum multiscale entanglement renormalization ansatz (cMERA). Given the ground state of a Chern insulator, we construct and study its cMERA by paying attention, in particular, to how the bulk holographic geometry and the Berry curvature depend on the topological properties of the ground state. It is found that each state defined at different energy scale of cMERA carries a nonzero Berry flux, which is emanated from the UV layer of cMERA, and flows towards the IR. Hence, a topologically nontrivial UV state flows under the renormalization group to an IR state, which is also topologically nontrivial. On the other hand, we found that there is an obstruction to construct the exact ground state of a topological insulator with a topologically trivial IR state. That is, if we try to construct a cMERA for the ground state of a Chern insulator by taking a topologically trivial IR state, the resulting cMERA does not faithfully reproduce the exact ground state at all length scales.

PHYSICAL REVIEW B 94[7] 075124, 2016. DOI: 10.1103/PhysRevB.94.075124

[P230-2016] "Influence of noble metals (Pd, Pt) on the performance of Ru/Al2O3 based catalysts for toluene hydrogenation in liquid phase"

Suppino, R. S.; **Landers, R.***; Gomez Cobo, A. J.

Catalytic hydrogenation of aromatic compounds is of great interest due to environmental aspects and the wide range of industrial processes involving such reaction. In this context, the present work aims to study the influence of Pd or Pt addition on the performance of Ru/Al2O3 based catalysts for toluene hydrogenation in liquid phase. For this, catalysts were prepared by wet impregnation from chlorinated precursors and reduced in liquid phase by formaldehyde (H2CO). After impregnation, a part of the catalysts were activated ex situ at 573 K or in situ at 523 K under H-2. The studied solids were characterized by N-2 physisorption, SEM + EDX, TEM, XPS and TPR techniques. Catalytic tests were conducted in a slurry Parr reactor at 373 K under constant H-2 pressure of 5 MPa. Results show that solids reduction by H2CO led to metallic species, while the activation treatments form oxides and decrease the catalytic activity. The initial reaction rate of non-activated monometallic catalysts follows the order: Ru/Al2O3 >> Pd/Al2O3 approximate to Pt/Al2O3. A synergistic effect on the activity of RU/Al2O3 based catalysts is induced by the Pt addition.

APPLIED CATALYSIS A-GENERAL 525, 41-49, 2016. DOI: 10.1016/j.apcata.2016.06.038

[P231-2016] "Kinetic Energy Release of the Singly and Doubly Charged Methylene Chloride Molecule: The Role of Fast Dissociation"

Alcantara, K. F.; Rocha, A. B.; **Gomes, A. H. A.***; Wolff, W.; Sigaud, L.; Santos, A. C. F.

The center of mass kinetic energy release distribution (KERD) spectra of selected ionic fragments, formed through dissociative single and double photoionization of CH2Cl2 at photon energies around the Cl 2p edge, were extracted from the shape and width of the experimentally obtained time-of flight (TOF) distributions. The KERD spectra exhibit either smooth profiles or structures, depending on the moiety and photon energy. In general, the heavier the ionic fragments, the lower their average KERDs are. In contrast, the light H+ fragments are observed-with kinetic energies centered around 4.5-5.5 eV, depending on the photon energy. It was observed that the change in the photon energy involves a change in the KERDs, indicating different processes or transitions taking place in the breakup process. In the particular case of double ionization with the ejection of two charged fragments, the KERDs present have characteristics compatible with the Coulombic fragmentation model. Intending to interpret the experimental data, singlet and triplet states at Cl 2p edge of the CH2Cl2 molecule, corresponding to the Cl (2p -> 10a(1)*) and Cl (2p -> 4b(1)*) transitions, were calculated at multiconfigurational self-consistent field (MCSCF) level and multireference configuration interaction (MRCI). These states were selected to form the spin orbit coupling matrix elements, which after diagonalization result in a spin orbit manifold.

Minimum energy pathways for dissociation of the molecule were additionally calculated aiming to give support to the presence of the ultrafast dissociation mechanism in the molecular breakup.

JOURNAL OF PHYSICAL CHEMISTRY A 120[34] 6728-6737, 2016. DOI: 10.1021/acs.jpca.6b05368

[P232-2016] "Lagrangian formulation of relativistic Israel--Stewart hydrodynamics"

Montenegro, D.*; Torrieri, G.*

We rederive relativistic hydrodynamics as a Lagrangian effective theory using the doubled coordinates technique, allowing us to include dissipative terms. We include Navier--Stokes shear and bulk terms, as well as Israel-Stewart relaxation time terms, within this formalism. We show how the inclusion of shear dissipation forces the inclusion of the Israel-Stewart term into the theory, thereby providing an additional justification for the form of this term.

PHYSICAL REVIEW D 94[6] 065042, 2016. DOI: 10.1103/PhysRevD.94.065042

[P233-2016] "Large extra dimensions at the Deep Underground Neutrino Experiment"

Berryman, J. M.; de Gouvea, A.; Kelly, K. J.; **Peres, O. L. G.***; Tabrizi, Z.

We investigate the potential of the long-baseline Deep Underground Neutrino Experiment (DUNE) to study large-extra--dimension (LED) models originally proposed to explain the smallness of neutrino masses by postulating that right-handed neutrinos, unlike all standard model fermion fields, can propagate in the bulk. The massive Kaluza-Klein (KK) modes of the right-handed neutrino fields modify the neutrino oscillation probabilities and can hence affect their propagation. We show that, as far as DUNE is concerned, the LED model is indistinguishable from a (3 + 3N)-neutrino framework for modest values of N; N = 1 is usually a very good approximation. Nonetheless, there are no new sources of CP-invariance violation other than one CP-odd phase that can be easily mapped onto the CP-odd phase in the standard three-neutrino paradigm. We analyze the sensitivity of DUNE to the LED framework and explore the capability of DUNE to differentiate the LED model from the three--neutrino scenario and from a generic (3 + 1)-neutrino model.

PHYSICAL REVIEW D 94[3] 033006, 2016. DOI: 10.1103/PhysRevD.94.033006

[P234-2016] "Localization transition in one dimension using Wegner flow equations"

Quito, V. L.*; Titum, P.; Pekker, D.; Refael, G.

The flow-equation method was proposed by Wegner as a technique for studying interacting systems in one dimension. Here, we apply this method to a disordered one-dimensional model with power-law decaying hoppings. This model presents a transition as function of the decaying exponent alpha. We derive the flow equations and the evolution of single-particle operators. The flow equation reveals the delocalized nature of the states for alpha < 1/2. Additionally, in the regime alpha > 1/2, we present a strong-bond renormalization group structure based on iterating the three-site clusters, where we solve the flow equations perturbatively. This renormalization group approach allows us to probe the critical point (alpha = 1). This method correctly reproduces the critical level-spacing statistics and the fractal dimensionality of the eigenfunctions.

PHYSICAL REVIEW B 94[10] 104202, 2016. DOI: 10.1103/PhysRevB.94.104202

[P235-2016] "Magnetic nanoparticles of Ni/NiO nanostructured in film form synthesized by dead organic matrix of yeast"

Salvadori, M. R.; Ando, R. A.; **Muraca, D.*; Knobel, M.***; Oller Nascimento, C. A.; Correa, B.

An innovative sustainable protocol of nanobiotechnology has been developed to synthesize Ni/NiO magnetic nanoparticles, nanostructured in film form, through a dead organic matrix of the yeast Rhodotorula mucilaginosa, which was isolated from the Amazon region. It is a synergistic strategy that utilizes green technology, thus minimizing environmental impact and reducing costs. The best conditions for the adsorption of the metal through the dead organic matrix and subsequent synthesis of the nanoparticles were monitored by analyzing the biosorption of nickel by the yeast. The structural characteristics of the film-forming nanoparticles were investigated via high-resolution transmission electron microscopy (HRTEM), atomic force microscopy (AFM), X-ray photoelectron spectroscopy (XPS), and infrared spectroscopy (FTIR). The magnetic properties of the nanoparticles produced by the dead organic matrix were determined in a superconducting quantum interference device (SQUID). Results indicate that the Ni/NiO nanoparticles are mainly spherical, with an average size of 5.5 nm, present magnetic properties, synthesized extracellularly and involve the proteins of the yeast, which probably confer organization in the film form. Such natural bioprocess suggests a rational protocol strategy as a template for the industrial--scale synthesis of magnetic nanoparticles of metals from the dead organic matrix of yeast and also provides a possible green system of nanobioremediation of metals from wastewater.

RSC ADVANCES 6[65] 60683-60692, 2016. DOI: 10.1039/c6ra07274g

[P236-2016] "Measurement of D-meson production versus multiplicity in p-Pb collisions at root s(NN)=5.02 TeV"

Adam, J.; Adamova, D.; Aggarwal, M. M.; **Chinellato, D. D.*; Dash, A.*; de Souza, R. D.*; Takahashi, J.***; et al.
ALICE Collaboration

The measurement of prompt D-meson production as a function of multiplicity in p-Pb collisions at TeV with the ALICE detector at root s(NN) the LHC is reported. D-0, D+ and Dau+ mesons are reconstructed via their hadronic decay channels in the centre-of-mass rapidity range -0.96 < y(cms) < 0.04 and transverse momentum interval 1 < p(T) < 24 GeV/c. The multiplicity dependence of D-meson production is examined by either comparing yields in p-Pb collisions in different event classes, selected based on the multiplicity of produced particles or zero-degree energy, with those in pp collisions, scaled by the number of binary nucleon-nucleon collisions (nuclear modification factor); as well as by evaluating the per-event yields in p-Pb collisions in different multiplicity intervals normalised to the multiplicity-integrated ones (relative yields). The nuclear modification factors for D-0, D+ and D*(+) are consistent with one another. The D-meson nuclear modification factors as a function of the zero-degree energy are consistent with unity within uncertainties in the measured p(T) regions and event classes. The relative D-meson yields, calculated in various p(T) intervals, increase as a function of the charged-particle multiplicity. The results are compared with the equivalent pp measurements at root s = 7 TeV as well as with EPOS 3 calculations.

JOURNAL OF HIGH ENERGY PHYSICS 8,078, 2016. DOI: 10.1007/JHEP08(2016)078

[P237-2016] "Measurement of inclusive jet production and nuclear modifications in pPb collisions at root s(NN)=5.02 TeV"

Khachatryan, V.; Sirunyan, A. M.; Tumasyan, A.; **Chinellato, J. A.*; Tonelli Manganote, E. J.***; et al.
CMS Collaboration

Inclusive jet production in pPb collisions at a nucleon-nucleon (NN) center-of-mass energy of root s(NN) = 5.02 TeV is studied with the CMS detector at the LHC. A data sample corresponding to an integrated luminosity of 30.1 nb(-1) is analyzed. The jet transverse momentum spectra are studied in seven pseudorapidity intervals covering the range -2.0 < eta(CM) < 1.5 in the NN center-of-mass frame. The jet production yields at forward and backward pseudorapidity are compared and no significant asymmetry about eta(CM) = 0 is observed in the measured kinematic range. The measurements in the pPb system are compared to reference jet spectra obtained by extrapolation from previous measurements in pp collisions at root s = 7 TeV. In all pseudorapidity ranges, nuclear modifications in inclusive jet production are found to be small, as predicted by next-to-leading order perturbative QCD calculations that incorporate nuclear effects in the parton distribution functions.

EUROPEAN PHYSICAL JOURNAL C 76[7]372, 2016. DOI: 10.1140/epjc/s10052-016-4205-7

[P238-2016] "Measurement of t(t)over-bar production with additional jet activity, including b quark jets, in the dilepton decay channel using pp collisions at root s=8TeV"

Khachatryan, V.; Sirunyan, A. M.; Tumasyan, A.; **Chinellato, J.*; Tonelli Manganote, E. J. A.***; et al.
CMS Collaboration

Jet multiplicity distributions in top quark pair (t (t) over bar) events are measured in pp collisions at a centre-of-mass energy of 8 TeV with the CMS detector at the LHC using a data set corresponding to an integrated luminosity of 19.7 fb(-1). The measurement is performed in the dilepton decay channels (e(+)e(-), mu(+)mu(-), and e(+/-)mu(+/-)). The absolute and normalized differential cross sections for t (t) over bar production are measured as a function of the jet multiplicity in the event for different jet transverse momentum thresholds and the kinematic properties of the leading additional jets. The differential t (t) over barb and t (t) over barb (b) over bar cross sections are presented for the first time as a function of the kinematic properties of the leading additional b jets. Furthermore, the fraction of events without additional jets above a threshold is measured as a function of the transverse momenta of the leading additional jets and the scalar sum of the transverse momenta of all additional jets. The data are compared and found to be consistent with predictions from several perturbative quantum chromodynamics event generators and a next-to-leading order calculation.

EUROPEAN PHYSICAL JOURNAL C 76[7]379, 2016. DOI: 10.1140/epjc/s10052-016-4105-x

[P239-2016] "Measurement of the differential cross sections for top quark pair production as a function of kinematic event variables in pp collisions at root s=7 and 8 TeV"

Khachatryan, V.; Sirunyan, A. M.; Tumasyan, A.; **Chinellato, J. A.*; Tonelli Manganote, E. J.***; et al.
CMS Collaboration

Measurements are reported of the normalized differential cross sections for top quark pair production with respect to four kinematic event variables: the missing transverse energy; the scalar sum of the jet transverse momentum (p(T)); the scalar sum of the pT of all objects in the event; and the pT of leptonically decaying W bosons from top quark decays. The data sample, collected using the CMS detector at the LHC, consists of 5.0 fb(-1) of proton-proton collisions at root s = 7 TeV and 19.7 fb(-1) at root s = 8 TeV. Top quark pair events containing one electron or muon are selected. The results are presented after correcting for detector effects to allow direct comparison with theoretical predictions. No significant deviations from the predictions of several standard model event simulation generators are observed.

PHYSICAL REVIEW D 94[5] 052006, 2016. DOI: 10.1103/PhysRevD.94.052006

[P240-2016] "Measurement of the Z gamma -> nu(nu)over--bar gamma production cross section in pp collisions at root s=8 TeV and limits on anomalous ZZ gamma and Z gamma gamma trilinear gauge boson couplings"

Khachatryan, V.; Sirunyan, A. M.; Tumasyan, A.; **Chinellato, D. D.*; Dash, A.*; de Souza, R. D.*; Takahashi, J.***; et al.
CMS Collaboration

An inclusive measurement of the Z gamma -> nu(nu) over bar gamma production cross section in pp collisions at root s = 8 TeV is presented, using data corresponding to an integrated luminosity of 19.6fb(-1) collected with the CMS detector at the LHC. This measurement is based on the observation of events with large missing energy and with a single photon with transverse momentum above 145 GeV and absolute pseudorapidity in the range vertical bar eta vertical bar < 1.44. The measured Z gamma -> nu<(nu)over bar>gamma production cross section, 52.7 +/- 2.1(stat) +/- 6.4(syst) +/- 1.4(lumi) fb, agrees well with the standard model prediction of 50.0(-2.2)(+2.4) fb. A study of the photon transverse momentum spectrum yields the most stringent limits to date on the anomalous ZZ gamma and Z gamma gamma trilinear gauge boson couplings.

PHYSICS LETTERS B 760, 448-468, 2016. DOI: 10.1016/j.physletb.2016.06.080

[P241-2016] "Measurement of transverse energy at midrapidity in Pb-Pb collisions at root s(NN)=2.76 TeV"

Adam, J.; Adamova, D.; Aggarwal, M. M.; **Albuquerque, D. S. D.*; Chinellato, D. D.*; de Souza, R. D.*; Takahashi, J.*;** ALICE Collaboration

We report the transverse energy (ET) measured with ALICE at midrapidity in Pb-Pb collisions at root s(NN) = 2.76 TeV as a function of centrality. The transverse energy was measured using identified single-particle tracks. The measurement was cross checked using the electromagnetic calorimeters and the transverse momentum distributions of identified particles previously reported by ALICE. The results are compared to theoretical models as well as to results from other experiments. The mean ET per unit pseudorapidity (eta), < dE(T)/d eta >, in 0%-5% central collisions is 1737 +/- 6(stat.) +/- 97(sys.) GeV. We find a similar centrality dependence of the shape of < dE(T)/d eta > as a function of the number of participating nucleons to that seen at lower energies. The growth in < dE(T)/d eta > at the LHC energies exceeds extrapolations of low-energy data. We observe a nearly linear scaling of < dE(T)/d eta > with the number of quark participants. With the canonical assumption of a 1 fm/c formation time, we estimate that the energy density in 0%-5% central Pb-Pb collisions at root s(NN) = 2.76 TeV is 12.3 +/- 1.0 GeV/fm(3) and that the energy density at the most central 80 fm(2) of the collision is at least 21.5 +/- 1.7 GeV/fm(3). This is roughly 2.3 times that observed in 0%-5% central Au-Au collisions at root s(NN) = 200 GeV.

PHYSICAL REVIEW C 94[3] 034903, 2016. DOI: 10.1103/PhysRevC.94.034903

[P242-2016] "Measurements of t(t)over-bar charge asymmetry using dilepton final states in pp collisions at root s=8 TeV"

Khachatryan, V.; Sirunyan, A. M.; Tumasyan, A.; **Chinellato, D. D.*; Dash, A.*; de Souza, R. D.*; Takahashi, J.***; et al.
CMS Collaboration

The charge asymmetry in ttevents is measured using dilepton final states produced in ppcollisions at the LHC at root s = 8 TeV. The data sample, collected with the CMS detector, corresponds to an integrated luminosity of 19.5 fb(-1). The measurements are performed using events with two oppositely charged leptons (electrons or muons) and two or more jets, where at least one of the jets is identified as originating from a bottom quark. The charge asymmetry is measured from differences in kinematic distributions, unfolded to the parton level, of positively and negatively charged top quarks and leptons. The t (t) over bar and leptonic inclusive charge asymmetries are found to be 0.011 +/- 0.011 (stat) +/- 0.007 (syst) and 0.003 +/- 0.006 (stat) +/- 0.003 (syst), respectively. These results, as well as charge asymmetry measurements made as a function of the invariant mass, rapidity, and transverse momentum of the t (t) over bar system, are in agreement with predictions of the standard model.

PHYSICS LETTERS B 760, 365-386, 2016. DOI: 10.1016/j.physletb.2016.07.006

[P243-2016] "Multiplicity dependence of charged pion, kaon, and (anti)proton production at large transverse momentum in p-Pb collisions root S-NN=5.02 TeV"

Adam, J.; Adamova, D.; Aggarwal, M. M.; **Chinellato, D. D.*; Dash, A.*; de Souza, R. D.*; Takahashi, J.***; et al.
ALICE Collaboration

The production of charged pions, kaons and (anti)protons has been measured at mid-rapidity (-0.5 < y < 0) in p-Pb collisions at root s(NN) = 5.02 TeV using the ALICE detector at the LHC. Exploiting particle identification capabilities at high transverse momentum (p(T)), the previously published p(T) spectra have been extended to include measurements up to 20 GeV/c for seven event multiplicity classes. The p(T) spectra for pp collisions at = 7 TeV, needed to interpolate a pp reference spectrum, have also been extended up to 20 GeV/c to measure the nuclear modification factor (R-ppb) in non-single diffractive p-Pb collisions. At intermediate transverse momentum (2 < p(T) < 10 GeV/c) the proton-to-pion ratio increases with multiplicity in p-Pb collisions, a similar effect is not present in the kaon-to-pion ratio. The p(T) dependent structure of such increase is qualitatively similar to those observed in pp and heavy-ion collisions. At high p(T) (>10 GeV/c), the particle ratios are consistent with those reported for pp and Pb--Pb collisions at the LHC energies. At intermediate p(T) the (anti)proton R-ppb shows a Cronin-like enhancement, while pions and kaons show little or no nuclear modification. At high p(T) the charged pion, kaon and (anti)proton R-ppb are consistent with unity within statistical and systematic uncertainties.

PHYSICS LETTERS B 760, 720-735, 2016. DOI: 10.1016/j.physletb.2016.07.050

[P244-2016] "Multitask Imidazolium Salt Additives for Innovative Poly(L-lactide) Biomaterials: Morphology Control, Candida spp. Biofilm Inhibition, Human Mesenchymal Stem Cell Biocompatibility, and Skin Tolerance"

Schrekker, C. M. L.; Sokolovicz, Y. C. A.; Raucci, M. G.; Selukar, B. S.; Klitzke, J. S.; Lopes, W.; Leal, C. A. M.; de Souza, I. O. P.; Galland, G. B.; dos Santos, J. H. Z.; Mauler, R. S.; Kol, M.; Dagorne, S.; Ambrosio, L.; Teixeira, M. L.; Morais, J.; **Landers, R.***; Fuentefria, A. M.; Schrekker, H. S.

Candida species have great ability to colonize and form biofilms on medical devices, causing infections in human hosts. In this study, poly(L-lactide) films with different imidazolium salt (1-n--hexadecyl-3-methylimidazolium chloride (C(16)MImCl) and 1-n--hexadecyl-3-methylimidazolium methanesulfonate (C(16)MImMeS)) contents were prepared, using the solvent casting process. Poly(L-lactide)-imidazolium salt films were obtained with different surface morphologies (spherical and directional), and the presence of the imidazolium salt in the surface was confirmed. These films with different concentrations of the imidazolium salts C(16)MImCl and C(16)MImMeS presented antibiofilm activity against isolates of Candida tropicalis, Candida parapsilosis, and Candida albicans. The minor antibiofilm concentration assay enabled one to determine that an increasing imidazolium salt content promoted, in general, an increase in the inhibition percentage of biofilm formation. Scanning electron microscopy micrographs confirmed the effective prevention of biofilm formation on the imidazolium salt containing biomaterials. Lower concentrations of the imidazolium salts showed no cytotoxicity, and the poly(L-lactide)-imidazolium salt films presented good cell adhesion and proliferation percentages with human mesenchymal stem cells. Furthermore, no acute microscopic lesions were identified in the histopathological evaluation after contact between the films and pig ear skin. In combination with the good morphological, physicochemical, and mechanical properties, these poly(L-lactide)-based materials with imidazolium salt additives can be considered as promising biomaterials for use in the manufacturing of medical devices.

ACS APPLIED MATERIALS & INTERFACES 8[33], 21163-21176, 2016. DOI: 10.1021/acsami.6b06005

[P245-2016] "Nanowire Arrays as Cell Force Sensors To Investigate Adhesin-Enhanced Holdfast of Single Cell Bacteria and Biofilm Stability"

Sahoo, P. K.*; Janissen, R.*; Monteiro, M. P.*; Cavalli, A.; **Murillo, D. M.***; Merfa, M. V.; **Cesar, C. L.***; Carvalho, H. F.; de Souza, A. A.; Bakkers, E. P. A. M.; **Cotta, M. A.***

Surface attachment of a planktonic bacteria, mediated by adhesins and extracellular polymeric substances (EPS), is a crucial step for biofilm formation. Some pathogens can modulate cell adhesiveness, impacting host colonization and virulence. A framework able to quantify cell-surface interaction forces and their dependence on chemical surface composition may unveil adhesiveness control mechanisms as new targets for intervention and disease control. Here we employed InP nanowire arrays to dissect factors involved in the early stage biofilm formation of the phytopathogen Xylella fastidiosa. Ex vivo experiments demonstrate single-cell adhesion forces up to 45 nN, depending on the cell orientation with respect to the surface. Larger adhesion forces occur at the cell poles; secreted EPS layers and filaments provide additional mechanical support. Significant adhesion force enhancements were observed for single cells anchoring a biofilm and particularly on XadA1 adhesincoated surfaces, evidencing molecular mechanisms developed by bacterial pathogens to create a stronger holdfast to specific host tissues.

NANO LETTERS 16[7] 4656-4664, 2016. DOI: 10.1021/acs.nanolett.6b01998

[P246-2016] "Neutrino mixing in accelerated proton decays"

Ahluwalia, D. Vir; Labun, L.; **Torrieri, G.***

We discuss the inverse beta-decay of accelerated protons in the context of neutrino flavor superpositions (mixings) in mass eigenstates. The process p -> nl(+) v(l) is kinematically allowed because the accelerating field provides the rest energy difference between initial and final states.

The rate of p -> n conversions can be evaluated in either the laboratory frame (where the proton is accelerating) or the co-moving frame (where the proton is at rest and interacts with an effective thermal bath of l and v(l) due to the Unruh effect). By explicit calculation, we show that the rates in the two frames disagree when taking into account neutrino mixings, because the weak interaction couples to charge eigenstates whereas gravity couples to neutrino mass eigenstates (D.V. Ahluwalia et al., arXiv:1505.04082 [hep-ph]). The contradiction could be resolved experimentally, potentially yielding new information on the origins of neutrino masses.

EUROPEAN PHYSICAL JOURNAL A 52[7]189, 2016. DOI: 10.1140/epja/i2016-16189-7

[P247-2016] "Optical and magnetic nanocomposites containing Fe3O4@SiO2 grafted with Eu3+ and Tb3+ complexes"

Khan, L. U.; **Muraca, D.***; Brito, H. F.; **Moscoso-Londono, O.***; Felinto, M. C. F. C.; **Pirota, K. R.***; Teotonio, E. E. S.; Malta, O. L.

The fabrication of bifunctional nanocomposites, co-assembling photonic (RE3+) and magnetic (Fe3O4) features into single entity nanostructures is reported through a facile method, using Fe3O4 as core nanoparticles, which were coated with SiO2 shell and further grafted with Eu3+ and Tb3+ complexes. The sophisticated structural features and morphologies of the core-shell Fe3O4@SiO2-(TTA-RE-L) nanomaterials were studied by Small--angle X-ray Scattering. The core mean size D-SAXS ,shell thickness Delta R, cluster size xi and fractal dimension D-F were determined by fitting the experimental SAXS data, corroborating through Transmission Electron Microscopy images. The DC magnetic properties at temperatures of 2 and 300 K were explored in support to the structural conclusions from SAXS and TEM analyses. The magnetic contributions of the RE3+ ions to the magnetizations of the Eu3+ and Tb3+ nanocomposites were discussed. The photoluminescence properties of the Eu3+ and Tb3+ nanocomposites based on the emission spectral data and luminescence decay curves were studied. The experimental intensity parameters (Omega(lambda)), lifetimes (tau), emission quantum efficiencies (eta) as well as radiative (A(rad)) and non--radiative (A(nrad)) decay rates were calculated and discussed, in addition, the structural conclusions from the values of the 4f-4f intensity parameters in the case of the Eu3+ ion. These novel Eu3+ and Tb3+ nanocomposites may act as red and green emitting layers for magnetic and light converting molecular devices.

JOURNAL OF ALLOYS AND COMPOUNDS 686, 453-466, 2016. DOI: 10.1016/j.jallcom.2016.06.009

[P248-2016] "Physical properties of Sr2FeIrO6 and Sr1.2La0.8FeIrO6 double perovskites obtained by a new synthesis route"

Bufaical, L.; Coutrim, L. T.; Santos, T. O.; **Terashita, H.*; Jesus, C. B. R.*; Pagliuso, P. G.***; Bittar, E. M.

Previous works on Sr2-xLaxFeIrO6 double perovskite (DP) series reported a possible ferromagnetic transition at T similar to 700 K for the x = 0.8 concentration, for which was observed the presence of spurious Fe2O3 phase. In order to prevent the formation of this impurity phase and check if this high temperature magnetic transition is intrinsic of the material, different synthesis routes became necessary. In this work, polycrystalline samples of Sr2-xLaxFeIrO6 (x = 0.0 and 0.8) have been synthesized by solid state reaction using a new heating treatment. The sample's properties were investigated by synchrotron x-ray powder diffraction (SXRD), transmission electron microscopy (TEM), magnetic susceptibility, specific heat and electrical resistivity, and compared with the previously reported results. The SXRD data revealed a structural transition induced by La to Sr substitution (I2/m <-> P2(1)/n). Moreover, it was not detected the presence of Fe2O3 on the samples obtained by the new route, which might be related to the absence of high temperature magnetic ordering. The magnetometry results indicated the emergence of Ir4+ with La doping, being corroborated by specific heat measurements which suggest Fe3+/Ir5+ and Fe3+/Ir4+ configurations for x = 0.0 and 0.8 compounds, respectively. Temperature dependent electrical resistivity measurements showed that Sr2+ to La3+ substitution leads to a decrease of electrical resistivity, possibly associated with the increase in the number of Ir valence electrons.

MATERIALS CHEMISTRY AND PHYSICS 182, 459-465, 2016. DOI: 10.1016/j.matchemphys.2016.07.057

[P249-2016] "Precursor anion states in dissociative electron attachment to chlorophenol isomers"

Kossoski, F.*; Varella, M. T. do N.

We report a theoretical study on low-energy (<10 eV) elastic electron scattering from chlorophenol isomers, namely, para--chlorophenol (pCP), meta-chlorophenol (mCP), and ortho--chlorophenol (oCP). The calculations were performed with the Schwinger multichannel method with pseudopotentials, and analysis of the computed integral cross sections and virtual orbitals revealed one sigma(CCl)*, one sigma(OH)*, and three pi* shape resonances. We show that electron capture into the two lower lying pi* orbitals initiates dissociative processes that lead to the elimination of the chloride ion, accounting for the two overlapping peaks where this fragment was observed. Despite the relatively small differences on the energetics of the pi* resonances, a major isomeric effect was found on their corresponding autodetachment lifetimes, which accounts for the observed increasing cross sections in the progression pCP < mCP < oCP. In particular, dissociation from the pi(1)* anion of pCP is largely suppressed because of the unfavorable mixing with the sigma(CCl)* state. We found the intramolecular hydrogen bond present in oCP to have the opposite effects of stabilizing the sigma(CCl)* resonance and destabilizing the sigma(OH)* resonance. We also suggest that the hydrogen abstraction observed in chlorophenols and phenol actually takes place by a mechanism in which the incoming electron is directly attached to the dissociative sigma(OH)* orbital.

JOURNAL OF CHEMICAL PHYSICS 145[4] 044310, 2016. DOI: 10.1063/1.4959229

[P250-2016] "Random SU(2)-symmetric spin-S chains"

Quito, V. L.*; Hoyos, J. A.; **Miranda, E.***

We study the low-energy physics of a broad class of time-reversal invariant and SU(2)-symmetric one-dimensional spin-S systems in the presence of quenched disorder via a strong--disorder renormalization-group technique. We show that, in general, there is an antiferromagnetic phase with an emergent SU(2S + 1) symmetry. The ground state of this phase is a random singlet state in which the singlets are formed by pairs of spins. For integer spins, there is an additional antiferromagnetic phase which does not exhibit any emergent symmetry (except for S = 1). The corresponding ground state is a random singlet one but the singlets are formed mostly by trios of spins. In each case the corresponding low-energy dynamics is activated, i.e., with a formally infinite dynamical exponent, and related to distinct infinite-randomness fixed points. The phase diagram has two other phases with ferromagnetic tendencies: a disordered ferromagnetic phase and a large spin phase in which the effective disorder is asymptotically finite. In the latter case, the dynamical scaling is governed by a conventional power law with a finite dynamical exponent.

PHYSICAL REVIEW B 94[6] 064405, 2016. DOI: 10.1103/PhysRevB.94.064405

[P251-2016] "Readout electronics validation and target detector assessment for the Neutrinos Angra experimente"

Alvarenga, T. A.; Anjos, J. C.; Azzi, G.; Cerqueira, A. S.; Chimenti, P.; Costa, J. A.; Dornelas, T. I.; Farias, P. C. M. A.; Guedes, G. P.; **Gonzalez, L. F. G.*; Kemp, E.***; Lima, H. P., Jr.; Machado, R.; Nobrega, R. A.; Pepe, I. M.; Ribeiro, D. B. S.; Simas Filho, E. F.; Valdiviesso, G. A.; Wagner, S.

A compact surface detector designed to identify the inverse beta decay interaction produced by anti-neutrinos coming from near operating nuclear reactors is being developed by the Neutrinos Angra Collaboration. In this document we describe and test the detector and its readout system by means of cosmic rays acquisition. In this measurement campaign, the target detector has been equipped with 16 8-in PMTs and two scintillator paddles have been used to trigger cosmic ray events. The achieved results disclosed the main operational characteristics of the Neutrinos Angra system and have been used to assess the detector and to validate its readout system.

NUCLEAR INSTRUMENTS & METHODS IN PHYSICS RESEARCH SECTION A-ACCELERATORS SPECTROMETERS DETECTORS AND ASSOCIATED EQUIPMENT 830, 206-213, 2016. DOI: 10.1016/j.nima.2016.05.052

[P252-2016] "RehabGesture: An Alternative Tool for Measuring Human Movement"

Brandao, A. F.; Dias, D. R. C.; **Castellano, G.***; Parizotto, N. A.; Trevelin, L. C.

Background: Systems for range of motion (ROM) measurement such as OptoTrak, Motion Capture, Motion Analysis, Vicon, and Visual 3D are so expensive that they become impracticable in public health systems and even in private rehabilitation clinics. Telerehabilitation is a branch within telemedicine intended to offer ways to increase motor and/or cognitive stimuli, aimed at faster and more effective recovery of given disabilities, and to measure kinematic data such as the improvement in ROM. Materials and Methods: In the development of the RehabGesture tool, we used the gesture recognition sensor Kinect (R) (Microsoft, Redmond, WA) and the concepts of Natural User Interface and Open Natural Interaction. Results: RehabGesture can measure and record the ROM during rehabilitation sessions while the user interacts with the virtual reality environment. The software allows the measurement of the ROM (in the coronal plane) from 0 degrees extension to 145 degrees flexion of the elbow joint, as well as from 0 degrees adduction to 180 degrees abduction of the glenohumeral (shoulder) joint, leaving the standing position. The proposed tool has application in the fields of training and physical evaluation of professional and amateur athletes in clubs and gyms and may have application in rehabilitation and physiotherapy clinics for patients with compromised motor abilities. Conclusions: RehabGesture represents a low-cost solution to measure the movement of the upper limbs, as well as to stimulate the process of teaching and learning in disciplines related to the study of human movement, such as kinesiology.

TELEMEDICINE AND E-HEALTH 22[7] 584-589, 2016. DOI: 10.1089/tmj.2015.0139

[P253-2016] "Resting state connectivity patterns with near-infrared spectroscopy data of the whole head"

Novi, S. L.*; Rodrigues, R. B. M. L.*; Mesquita, R. C.*

Resting state cerebral dynamics has been a useful approach to explore the brain's functional organization. In this study, we employed graph theory to deeply investigate resting state functional connectivity (rsFC) as measured by near-infrared spectroscopy (NIRS). Our results suggest that network parameters are very similar across time and subjects. We also identified the most frequent connections between brain regions and the main hubs that participate in the spontaneous activity of brain hemodynamics. Similar to previous findings, we verified that symmetrically located brain areas are highly connected. Overall, our results introduce new insights in NIRS-based functional connectivity at rest.

BIOMEDICAL OPTICS EXPRESS 7[7] 2524-2537, 2016. DOI: 10.1364/BOE.7.002524

[P254-2016] "Scaling in heavy-ion collisions and the low-energy frontier"

Torrieri, G.*

The common interpretation of elliptic flow v(2) in heavy-ion collisions is that it is produced by hydrodynamic flow at low transverse momentum and by parton energy loss at high transverse momentum. Here, we discuss this interpretation in view of the dependence of v(2) on energy, rapidity and system size, and show that it is far from clear how the relevant properties necessary for this interpretation, low viscosity and high opacity, turn on. A low-energy collider such as NICA is essential for this interpretation to be verified, understood and related to the fundamental properties of hadronic matter.

EUROPEAN PHYSICAL JOURNAL A 52[8] 249, 2016. DOI: 10.1140/epja/i2016-16249-0

[P255-2016] "Search for Higgs boson off-shell production in proton-proton collisions at 7 and 8 TeV and derivation of constraints on its total decay width"

Khachatryan, V.; Sirunyan, A. M.; Tumasyan, A.; **Chinellato, J. A.*; Tonelli Manganote, E. J.***; et al.
CMS Collaboration

A search is presented for the Higgs boson off-shell production in gluon fusion and vector boson fusion processes with the Higgs boson decaying into a W+W- pair and the W bosons decaying leptonically. The data observed in this analysis are used to constrain the Higgs boson total decay width. The analysis is based on the data collected by the CMS experiment at the LHC, corresponding to integrated luminosities of 4.9 fb(-1) at a centre-of-mass energy of 7 TeV and 19.4 fb(-1) at 8 TeV, respectively. An observed (expected) upper limit on the off-shell Higgs boson event yield normalised to the standard model prediction of 2.4 (6.2) is obtained at the 95% CL for the gluon fusion process and of 19.3 (34.4) for the vector boson fusion process. Observed and expected limits on the total width of 26 and 66 MeV are found, respectively, at the 95% confidence level (CL). These limits are combined with the previous result in the ZZ channel leading to observed and expected 95% CL upper limits on the width of 13 and 26 MeV, respectively.

JOURNAL OF HIGH ENERGY PHYSICS 9, 051, 2016. DOI: 10.1007/JHEP09(2016)051

[P256-2016] "Search for Narrow Resonances in Dijet Final States at root s=8 TeV with the Novel CMS Technique of Data Scouting"

Khachatryan, V.; Sirunyan, A. M.; Tumasyan, A.; **Chinellato, J. A.*; Tonelli Manganote, E. J.***; et al.
CMS Collaboration

A search for narrow resonances decaying into dijet final states is performed on data from proton-proton collisions at a center--of-mass energy of 8 TeV, corresponding to an integrated luminosity of 18.8 fb(-1). The data were collected with the CMS detector using a novel technique called data scouting, in which the information associated with these selected events is much reduced, permitting collection of larger data samples. This technique enables CMS to record events containing jets at a rate of 1 kHz, by collecting the data from the high-level-trigger system. In this way, the sensitivity to low-mass resonances is increased significantly, allowing previously inaccessible couplings of new resonances to quarks and gluons to be probed. The resulting dijet mass distribution yields no evidence of narrow resonances. Upper limits are presented on the resonance cross sections as a function of mass, and compared with a variety of models predicting narrow resonances. The limits are translated into upper limits on the coupling of a leptophobic resonance Z'(B) to quarks, improving on the results obtained by previous experiments for the mass range from 500 to 800 GeV.

PHYSICAL REVIEW LETTERS 117[3]031802, 2016. DOI: 10.1103/PhysRevLett.117.031802

[P257-2016] "Search for R-parity violating decays of a top squark in proton-proton collisions at root s=8TeV"

Khachatryan, V.; Sirunyan, A. M.; Tumasyan, A.; **Chinellato, D. D.*; Dash, A.*; de Souza, R. D.*; Takahashi, J.***; et al.
CMS Collaboration

The results of a search for a supersymmetric partner of the top quark (top squark), pair-produced in proton-proton collisions at root s = 8 TeV, are presented. The search, which focuses on R-parity violating, chargino-mediated decays of the top squark, is performed in final states with low missing transverse momentum, two oppositely charged electrons or muons, and at least five jets. The analysis uses a data sample corresponding to an integrated luminosity of 19.7 fb(-1)collected with the CMS detector at the LHC in 2012. The data are found to be in agreement with the standard model expectation, and upper limits are placed on the top squark pair production cross section at 95% confidence level. Assuming a 100% branching fraction for the top squark decay chain, (t) over tilde -> t (chi) over tilde (+/-)(1), (chi) over tilde (+/-)(1) -> l(+/-) + jj, top squark masses less than 890(1000) GeV for the electron (muon) channel are excluded for the first time in models with a single nonzero R-parity violating coupling. lambda'(ijk) (i, j, k <= 2), where i, j, k correspond to the three generations.

PHYSICS LETTERS B 760, 178-201, 2016. DOI: 10.1016/j.physletb.2016.06.039

[P258-2016] "Search for Resonant Production of High-Mass Photon Pairs in Proton-Proton Collisions at root s=8 and 13 TeV"

Khachatryan, V.; Sirunyan, A. M.; Tumasyan, A.; **Chinellato, J. A.*; Tonelli Manganote, E. J.***; et al.
CMS Collaboration

A search for the resonant production of high-mass photon pairs is presented. The analysis is based on samples of proton-proton collision data collected by the CMS experiment at center-of-mass energies of 8 and 13 TeV, corresponding to integrated luminosities of 19.7 and 3.3 fb(-1), respectively. The interpretation of the search results focuses on spin-0 and spin-2 resonances with masses between 0.5 and 4 TeV and with widths, relative to the mass, between 1.4 x 10(-4) and 5.6 x 10(-2). Limits are set on scalar resonances produced through gluon-gluon fusion, and on Randall-Sundrum gravitons. A modest excess of events compatible with a narrow resonance with a mass of about 750 GeV is observed. The local significance of the excess is approximately 3.4 standard deviations. The significance is reduced to 1.6 standard deviations once the effect of searching under multiple signal hypotheses is considered. More data are required to determine the origin of this excess.

PHYSICAL REVIEW LETTERS 117[5] 051802, 2016. DOI: 10.1103/PhysRevLett.117.051802

[P259-2016] "Search for s channel single top quark production in pp collisions at root s=7 and 8 TeV"

Khachatryan, V.; Sirunyan, A. M.; Tumasyan, A.; **Chinellato, J. A.*; Tonelli Manganote, E. J.***; et al.
CMS Collaboration

A search is presented for single top quark production in the s channel in proton-proton collisions with the CMS detector at the CERN LHC in decay modes of the top quark containing a muon or an electron in the final state. The signal is extracted through a maximum-likelihood fit to the distribution of a multivariate discriminant defined using boosted decision trees to separate the expected signal contribution from background processes. The analysis uses data collected at centre-of-mass energies of 7 and 8 TeV and corresponding to integrated luminosities of 5.1 and 19.7 fb(-1), respectively. The measured cross sections of 7.1 +/- 8.1 pb (at 7 TeV) and 13.4 +/- 7.3 pb (at 8 TeV) result in a best fit value of 2.0 +/- 0.9 for the combined ratio of the measured and expected values. The signal significance is 2.5 standard deviations, and the upper limit on the rate relative to the standard model expectation is 4.7 at 95% confidence level.

JOURNAL OF HIGH ENERGY PHYSICS 9, 027, 2016. DOI: 10.1007/JHEP09(2016)027

[P260-2016] "Search for the associated production of a Higgs boson with a single top quark in proton-proton collisions at root s=8 TeV"

Khachatryan, V.; Sirunyan, A. M.; Tumasyan, A.; **Chinellato, J. A.*; Tonelli Manganote, E. J.***; et al.
CMS Collaboration

This paper presents the search for the production of a Higgs boson in association with a single top quark (tHq), using data collected in proton-proton collisions at a center-of-mass energy of 8TeV corresponding to an integrated luminosity of 19.7 fb(-1). The search exploits a variety of Higgs boson decay modes resulting in final states with photons, bottom quarks, and multiple charged leptons, including tau leptons, and employs a variety of multivariate techniques to maximize sensitivity to the signal. The analysis is optimized for the opposite sign of the Yukawa coupling to that in the standard model, corresponding to a large enhancement of the signal cross section. In the absence of an excess of candidate signal events over the background predictions, 95% confidence level observed (expected) upper limits on anomalous tHq production are set, ranging between 600 (450) fb and 1000 (700) fb depending on the assumed diphoton branching fraction of the Higgs boson. This is the first time that results on anomalous tHq production have been reported.

JOURNAL OF HIGH ENERGY PHYSICS 6, 177, 2016. DOI: 10.1007/JHEP06(2016)177

[P261-2016] "Solid-Vapor Reaction Growth of Transition--Metal Dichalcogenide Monolayers"

Li, Bo; Gong, Y.; Hu, Z.; **Brunetto, G.***; Yang, Y.; Ye, G.; Zhang, Z.; Lei, S.; Jin, Z.; Bianco, E.; Zhang, X.; Wang, W.; Lou, J.; **Galvao, D. S.***; Tang, M.; Yakobson, B. I.; Vajtai, R.; Ajayan, P. M.

Two-dimensional (2D) layered semiconducting transition-metal dichalcogenides (TMDCs) are promising candidates for next-generation ultrathin, flexible, and transparent electronics. Chemical vapor deposition (CVD) is a promising method for their controllable, scalable synthesis but the growth mechanism is poorly understood. Herein, we present systematic studies to understand the CVD growth mechanism of monolayer MoSe2, showing reaction pathways for growth from solid and vapor precursors. Examination of metastable nanoparticles deposited on the substrate during growth shows intermediate growth stages and conversion of non-stoichiometric nanoparticles into stoichiometric 2D MoSe2 monolayers. The growth steps involve the evaporation and reduction of MoO3 solid precursors to sub-oxides and stepwise reactions with Se vapor to finally form MoSe2. The experimental results and proposed model were corroborated by abinitio Car-Parrinello molecular dynamics studies.

ANGEWANDTE CHEMIE-INTERNATIONAL EDITION 55[36] 10656-10661, 2016. DOI: 10.1002/anie.201604445

[P262-2016] "Strong, Twist-Stable Carbon Nanotube Yarns and Muscles by Tension Annealing at Extreme Temperatures"

Di, J.; Fang, S.; **Moura, F. A.*; Galvao, D. S.***; Bykova, J.; Aliev, A.; de Andrade, M. J.; Lepro, Li, Na; Haines, C.; Ovalle-Robles, R.; Qian, D.; Baughman, R. H.

A high-speed incandescent tension annealing process (ITAP) is used to increase the modulus and strength of twist-spun carbon nanotube yarns by up to 12-fold and 2.6-fold, respectively, provide remarkable resistance to oxidation and powerful protonating acids, and freeze yarn untwist. This twist stability enables torsional artificial-muscle motors having improved performance and minimizes problematic untwist during weaving nanotube yarns.

ADVANCED MATERIALS 28[31]6598-6605, 2016. DOI: 10.1002/adma.201600628

[P263-2016] "Suppression of Fermi acceleration in composite particles"

Siqueira, K. M.*; Aguiar, M. A. M.*

We study the motion of a composite particle in a one-dimensional billiard with a moving wall. The particle is modeled by two point masses coupled by a harmonic spring. We show that the energy gained by the composite particle is greatly reduced with respect to a single point particle. We show that the amount of energy transferred to the system at each collision with the walls is independent of the spring constant. However, the presence of the spring is responsible for the energy suppression because it diminishes the number of collisions by storing part of the system's energy and reducing the velocity of the particle's center of mass.

PHYSICA D-NONLINEAR PHENOMENA 331, 81-88, 2016. DOI: 10.1016/j.physd.2016.05.009

[P264-2016] "Surface and interface interplay on the oxidizing temperature of iron oxide and Au-iron oxide core-shell nanoparticles"

Sarveena; **Muraca, D.***; Zelis, P. M.; Javed, Y.; Ahmad, N.; Vargas, J. M.; **Moscoso-Londono, O.*; Knobel, M.***; Singh, M.; Sharma, S. K.

This article presents the effect of oxidation temperature on shape anisotropy, phase purity and growth of core-shell heterostructures and consequently their effect on structure-property relationships. Iron oxide and Au-iron oxide nanocomposites were synthesized by a thermal decomposition method by passing pure oxygen at different temperatures (125-250 degrees C). The prepared nanoparticles were surface functionalized by organic molecules; the presence of the organic canopy prevented both direct particle contact as well as further oxidation, resulting in the stability of the nanoparticles. We have observed a systematic improvement in the core and shell shape through tuning the reaction time as well as the oxidizing temperatures. Spherical and spherical triangular shaped core-shell structures have been obtained at an optimum oxidation temperature of 125 degrees C and 150 degrees C for 30 minutes. However, further increase in the temperature as well as oxidation time results in core-shell structure amendment and results in fully grown core-shell heterostructures. As stability and ageing issues limit the use of nanoparticles in applications, to ensure the stability of the prepared iron oxide nanoparticles we performed XRD analysis after more than a year and they remained intact showing no ageing effect. Specific absorption rate values useful for magnetic fluid hyperthermia were obtained for two samples on the basis of detailed characterization using X-ray diffraction, high-resolution transmission electron microscopy, Mossbauer spectroscopy, and dc-magnetization experiments.

RSC ADVANCES 6[74] 70394-70404, 2016. DOI: 10.1039/c6ra15610j

[P265-2016] "Synchrony-optimized networks of Kuramoto oscillators with inertia"

Pinto, R. S.*; Saa, A.

We investigate synchronization in networks of Kuramoto oscillators with inertia. More specifically, we introduce a rewiring algorithm consisting basically in a hill climb scheme in which the edges of the network are swapped in order to enhance its synchronization capacity. We show that the synchrony-optimized networks generated by our algorithm have some interesting topological and dynamical properties. In particular, they typically exhibit an anticipation of the synchronization onset and are more robust against certain types of perturbations. We consider synthetic random networks and also a network with a topology based on an approximated model of the (high voltage) power grid of Spain, since networks of Kuramoto oscillators with inertia have been used recently as simplified models for power grids, for which synchronization is obviously a crucial issue. Despite the extreme simplifications adopted in these models, our results, among others recently obtained in the literature, may provide interesting principles to guide the future growth and development of real-world grids, specially in the case of a change of the current paradigm of centralized towards distributed generation power grids.

PHYSICA A-STATISTICAL MECHANICS AND ITS APPLICATIONS 463, 77-87, 2016. DOI: 10.1016/j.physa.2016.07.009

[P266-2016] "Synthesis of ultralow density 3D graphene--CNT foams using a two-step method"

Vinod, S.; Tiwary, C. S.; **Machado, L. D.***; Ozden, S.; Vajtai, R.; **Galvao, D. S.***; Ajayan, P. M.

Here, we report a highly scalable two-step method to produce graphene foams with ordered carbon nanotube reinforcements. In our approach, we first used solution assembly methods to obtain graphene oxide foam. Next, we employed chemical vapor deposition to simultaneously grow carbon nanotubes and thermally reduce the 3D graphene oxide scaffold. The resulting structure presented increased stiffness, good mechanical stability and oil absorption properties. Molecular dynamics simulations were carried out to further elucidate failure mechanisms and to understand the enhancement of the mechanical properties.

The simulations showed that mechanical failure is directly associated with bending of vertical reinforcements, and that, for similar length and contact area, much more stress is required to bend the corresponding reinforcements of carbon nanotubes, thus explaining the experimentally observed enhanced mechanical properties.

NANOSCALE 8[35] 15857-15863, 2016. DOI: 10.1039/c6nr04252j

[P267-2016] "Thermoacoustic and thermoreflectance imaging of biased integrated circuits: Voltage and temperature maps"

Hernandez-Rosales, E.*; Cedeno, E.*; Hernandez-Wong, J.; Rojas-Trigos, J. B.; Marin, E.; **Gandra, F. C. G.*; Mansanares, A. M.***

In this work a combined thermoacoustic and thermoreflectance set-up was designed for imaging biased microelectronic circuits. In particular, it was used with polycrystalline silicon resistive tracks grown on a monocrystalline Si substrate mounted on a test chip. Thermoreflectance images, obtained by scanning a probe laser beam on the sample surface, clearly show the regions periodically heated by Joule effect, which are associated to the electric current distribution in the circuit. The thermoacoustic signal, detected by a pyroelectric/piezoelectric sensor beneath the chip, also discloses the Joule contribution of the whole sample. However, additional information emerges when a non-modulated laser beam is focused on the sample surface in a raster scan mode allowing imaging of the sample. The distribution of this supplementary signal is related to the voltage distribution along the circuit.

APPLIED PHYSICS LETTERS 109[4] 041902, 2016. DOI: 10.1063/1.4959828

[P268-2016] "Tilted excitation implies odd periodic resonances"

Depetri, G. I.*; Sartorelli, J. C.; Marin, B.; Baptista, M. S.

Our aim is to unveil how resonances of parametric systems are affected when symmetry is broken. We showed numerically and experimentally that odd resonances indeed come about when the pendulum is excited along a tilted direction. Applying the Melnikov subharmonic function, we not only determined analytically the loci of saddle-node bifurcations delimiting resonance regions in parameter space but also explained these observations by demonstrating that, under the Melnikov method point of view, odd resonances arise due to an extra torque that appears in the asymmetric case.

PHYSICAL REVIEW E 94[1] 012202, 2016. DOI: 10.1103/PhysRevE.94.012202

[P269-2016] "Unified description of seagull cancellations and infrared finiteness of gluon propagators"

Aguilar, A. C.*; Binosi, D.; **Figueiredo, C. T.***; Papavassiliou, J.

We present a generalized theoretical framework for dealing with the important issue of dynamical mass generation in Yang-Mills theories, and, in particular, with the infrared finiteness of the gluon propagators, observed in a multitude of recent lattice simulations. Our analysis is manifestly gauge invariant, in the sense that it preserves the transversality of the gluon self-energy, and gauge independent, given that the conclusions do not depend on the choice of the gauge-fixing parameter within the linear covariant gauges. The central construction relies crucially on the subtle interplay between the Abelian Ward identities satisfied by the nonperturbative vertices and a special integral identity that enforces a vast number of "seagull cancellations" among the one-and two--loop dressed diagrams of the gluon Schwinger-Dyson equation. The key result of these considerations is that the gluon propagator remains rigorously massless, provided that the vertices do not contain (dynamical) massless poles. When such poles are incorporated into the vertices, under the pivotal requirement of respecting the gauge symmetry of the theory, the terms comprising the Ward identities conspire in such a way as to still enforce the total annihilation of all quadratic divergences, inducing, at the same time, residual contributions that account for the saturation of gluon propagators in the deep infrared.

PHYSICAL REVIEW D 94[4] 045002, 2016. DOI: 10.1103/PhysRevD.94.045002

[P270-2016] "Unusual Kondo-hole effect and crystal-field frustration in Nd-doped CeRhIn5"

Rosa, P. F. S.; Oostra, A.; Thompson, J. D.; **Pagliuso, P. G.***; Fisk, Z.

We investigate single crystals of Ce1-xNdxRhIn5 by means of x-ray-diffraction, microprobe, magnetic susceptibility, heat capacity, and electrical resistivity measurements. Our data reveal that the antiferromagnetic transition of CeRhIn5, at T--N(Ce) = 3.8 K, is linearly suppressed with x(Nd). We associate this effect with the presence of a "Kondo hole" created by Nd substitution. The extrapolation of T-N(Ce) to zero temperature, however, occurs at x(c) similar to 0.3, which is below the two-dimensional percolation limit found in Ce1-xLaxRhIn5. This result strongly suggests the presence of a crystal-field induced magnetic frustration. Near x(Nd) similar to 0.2, the Ising antiferromagnetic order from Nd3+ ions is stabilized and T-N(Nd) increases up to 11 K in NdRhIn5. Our results shed light on the effects of magnetic doping in heavy-fermion antiferromagnets and stimulate the study of such systems under applied pressure.

PHYSICAL REVIEW B 94[4] 045101, 2016. DOI: 10.1103/PhysRevB.94.045101

[P271-2016] "Weak measurement of the composite Goos--Hanchen shift in the critical region"

Santana, O. J. S.*; Carvalho, S. A.; De Leo, S.; **de Araujo, L. E. E.***

By using a weak measurement technique, we investigated the interplay between the angular and the lateral Goos--Hanchen shift of a focused He-Ne laser beam for incidence near the critical angle. We verified that this interplay dramatically affects the composite Goos-Hanchen shift of the propagated beam. The experimental results confirm theoretical predictions that recently appeared in the literature.

OPTICS LETTERS 41[16] 3884-3887, 2016. DOI: 10.1364/OL.41.003884

[P272-2016] "Zero-phi(eff) non-Bragg gap solitons in 1D Kerr polaritonic/metamaterial heterostructures"

Reyes-Gomez, E.; Cavalcanti, S. B.; **Oliveira, L. E.***

A theoretical study of one-dimensional heterostructures composed of alternate layers of a Kerr polaritonic material and a linear dispersive metamaterial is performed. For frequency values at the edges of the non-Bragg zero--phi(eff) gap of the heterostructure in the linear regime,

a switching from very low to high transmission states is obtained and localized gap solitons of various orders are found, depending on the particular value of the incident power. Soliton solutions are shown to be robust with respect to absorption effects and a study is presented for gap soliton phases at the top and bottom of the zero-phi(eff) gap in the case of defocusing and focusing nonlinearities.

PHYSICA E-LOW-DIMENSIONAL SYSTEMS & NANOSTRUCTURES 83, 461-465, 2016. DOI: 10.1016/j.physe.2015.12.030

Eventos publicados

[P273-2016] "Effect of high-optical excitation on the ultrafast electron dynamics in stacked-monolayer graphene samples"

Castaneda, J. A.*; Rosa, H. G.; **Gomes, J. C. V.***; Thoroh de Souza, E. A.; **de Brito Cruz, C. H.*; Fragnito, H. L.*; Padilha, L. A.***

We report on transient absorption experiments performed at high optical excitation fluences and used to study the ultrafast dynamics in graphene. We employed a degenerated scheme of pump and probe at 800 nm (1.55 eV). The time resolution of our measurements was limited by the pulse duration similar to 100 fs. The samples were prepared by chemical vapor deposition (CVD) as single-layers on silica and, then staked layer-by-layer in order to make a stack of up to 5 graphene monolayers. We observed saturable absorption (SA) and fluence-dependent relaxation times. We see that the ultrafast carrier dynamics is composed by two decay mechanisms, one with response time of about 200 fs and a slower process of about 1 ps. The fast decay, due to both carrier-carrier and carrier-optical phonon scattering, becomes slower when the density of excited carrier was increased. We implemented a theoretical model and found that both the optical phonon rate emission and the optical phonon lifetime are affect by the pump fluence.

ULTRAFAST BANDGAP PHOTONICS (Proceedings of SPIE) 9835, UNSP 983517, 2016. DOI: 10.1117/12.2235501

Conference on Ultrafast Bandgap Photonics, Baltimore, MD. SPIE. APR 18-20, 2016.

[P274-2016] "Exchange bias field in mixed arrangement of NiO-Ni nanoparticles"

Sarveena; Kumar, S.; Singh, M.; **Sharma, S. K.***

Three samples of naturally mixed Ni (>120 nm) and NiO (similar to 10 nm) were prepared with different particle diameters/distributions and amount of metallic nickel. Exchange bias effect has been observed and strongly depends upon both particle sizes/distributions and concentration of Ni, achieving the highest value (similar to 2200 Oe at 5 K) for the pure NiO, while the corresponding value for the sample with maximum Ni concentration is similar to 70 Oe. This is tentatively explained taking into account the effect of induced dipolar field by bigger Ni particles on the stabilization of magnetically ordered surface regions of the smaller NiO nanoparticles.

DAE SOLID STATE PHYSICS SYMPOSIUM 20159 (AIP Conference Proceedings) 1731, 050115 DOI: 10.1063/1.4947769

DAE Solid State Physics Symposium, Amity Univ, Noida, INDIA. Board Res Nucl Sci, Dept Atom Energy. DEC 21-25, 2015.

Patentes

[Pa001-2016] "Processo de fabricação de peneiras submicrométricas e peneiras assim obtidas"

Lucila Helena Deliesposte Cescato; Luis Enrique Gutierrez Rivera; Edson José de Carvalho

Número da Patente ou Registro: Agência INOVA: PI0404934-9
Tipo: Patente de Invenção
Mês/Ano de Conclusão: 12/2015 - INPI/BBRASIL

[Pa002-2016] "Processo de obtenção de partículas semi-amorfas de sílica, partículas assim obtidas e seus usos"

Egont Alexandre Schenkel; Éric Fujiwara; Murilo Ferreira Marques dos Santos; Carlos Kenichi Suzuki

Número da Patente ou Registro: Agência INOVA: BR 10 2015 031934 7
Tipo: Patente de Invenção
Mês/Ano de Conclusão: 12/2015 - INPI/BBRASIL

[Pa003-2016] "Processo de preparação de vidros teluritos dopados com quantum dots de PbTe"

Luiz Carlos Barbosa; Carlos Lenz Cesar; Gilberto Júnior Jacob

Número da Patente ou Registro: Agência INOVA: PI0406092-0
Tipo: Patente de Invenção
Mês/Ano de Conclusão: 06/2015 - INPI/BBRASIL

Fonte: SIPEX - Sistema de Informação de Pesquisa e Extensão da Unicamp.

Livro Publicado

[L003-2016] "Reise in die DDR: Ein Blick von Außerhalb auf den Alltag der ehemaligen Deutschen Demokratischen Republik"

João de Góes

[s.l.] : Verlag Lebensreise, 2016. 88 páginas. ISBN: 978-3-639-82712-5

***Autores da comunidade IFGW**
Fonte: Web of Science on-line.

Defesas de Dissertações

[D022-2016] "Infrared Behavior of the Ghost-Gluon Vertex and its Implications"
Aluno: Antonio Maurício Soares Narciso
Orientador: Profa. Dra. Arlene Cristina Aguilar
Data: 30/09/2016

[D023-2016] "Estudos de "annealing" de traços de íons e traços de fissão em muscovita"
Aluno: Arnaldo Luis Lixandrão Filho
Orientador: Prof. Dr. Sandro Guedes de Oliveira
Data: 25/10/2016

Defesas de Teses

[T012-2016] "Atmospheric muonic lepton fluxes and their systematic uncertainties"
Aluno: Felipe Campos Penha
Orientador: Prof. Dr. Orlando Luis Goulart Peres
Data: 11/11/2016

[T013-2016] "Estudo de redução térmica, efusão de espécies e alterações estruturais em filmes finos de óxido de grafeno"
Aluno: Douglas Soares da Silva
Orientador: Prof. Dr. Francisco das Chagas Marques
Data: 24/11/2016

Fonte: Portal IFGW/Pós-graduação - Agenda de Colóquios, Defesas e Seminários.
Disponível em: http://portal.ifi.unicamp.br/pos-graduacao

Abstracta

Instituto de Física
Diretor: Prof. Dr. Newton Cesario Frateschi
Diretor Associado: Prof. Dr. Luís Eduardo Evangelista de Araujo
Universidade Estadual de Campinas - UNICAMP
Cidade Universitária Zeferino Vaz
13083-859 - Campinas - SP - Brasil
e-mail: secdir@ifi.unicamp.br

Publicação

Biblioteca do Instituto de Física Gleb Wataghin
http://portal.ifi.unicamp.br/biblioteca

Diretora Técnica: Sandra Maria Carlos Cartaxo
Coordenador da Comissão de Biblioteca: Prof. Dr. André Koch Torres de Assis

Elaboração
Maria Graciele Trevisan (Bibliotecária)
contato: infobif@ifi.unicamp.br